



Noninvasive evaluation of liver fibrosis: comparison of the stretched exponential diffusion-weighted model to other diffusion-weighted MRI models and transient elastography

Jae Hyon Park¹ · Nieun Seo¹ · Yong Eun Chung¹ · Seung Up Kim² · Yung Nyun Park³ · Jin-Young Choi¹ · Mi-Suk Park¹ · Myeong-Jin Kim¹

Received: 24 June 2020 / Revised: 18 November 2020 / Accepted: 3 December 2020 / Published online: 13 January 2021
© European Society of Radiology 2021

Abstract

Objectives To compare the diagnostic performance of the stretched exponential model to those of other DWI models and transient elastography (TE) and to evaluate the influence of confounding factors on the staging of liver fibrosis.

Methods This retrospective study included 78 consecutive patients who underwent both DWI and TE. The distributed diffusion coefficient (DDC) and intravoxel heterogeneity index (α) from the stretched exponential model, apparent diffusion coefficient (ADC), perfusion fraction (f), pseudodiffusion coefficient (D_p), true diffusion coefficient (D_t), and TE were obtained. Associations between imaging parameters and pathological fibrosis, inflammation, and steatosis were evaluated using Spearman's correlation and multiple regression analysis. Diagnostic accuracy of parameters for fibrosis staging was assessed via the Obuchowski measures.

Results DDC was the only parameter to differ between F0–1 and F2–3 ($p < 0.001$) and between F2–3 and F4 ($p = 0.013$). DDC showed significant correlation with fibrosis ($p < 0.001$) and inflammation ($p = 0.001$), but not with steatosis ($p = 0.619$), and was independently associated with only fibrosis in multiple regression analysis ($\beta = -0.114$, $p < 0.001$). ADC, D_p , and D_t showed a significant correlation with steatosis ($ps \leq 0.038$). DDC showed the highest diagnostic performance for liver fibrosis (0.717; 95% confidence interval, 0.653–0.765) followed by TE (0.681, 0.623–0.733) without a significant difference between DDC and TE ($p > 0.999$).

Conclusions DDC from the stretched exponential model is the most accurate DWI parameter with no confounding effect from steatosis and with overall similar diagnostic performance to TE.

Key Points

- The distributed diffusion coefficient (DDC) from the stretched exponential model is the most accurate DWI parameter for staging liver fibrosis.
- DDC and transient elastography have similar good diagnostic performance for evaluating liver fibrosis.
- The stretched exponential DWI model has no confounding effect by steatosis, unlike other DWI models.

Keywords Diffusion magnetic resonance imaging · Elasticity imaging techniques · Fibrosis · Liver

Abbreviations and acronyms

α Intravoxel diffusion heterogeneity index
 α^a α obtained using a four b -value dataset
ADC Apparent diffusion coefficient

D_p Pseudodiffusion coefficient
 D_t True diffusion coefficient
DDC Distributed diffusion coefficient
DDC^a DDC obtained using a four b -value dataset

✉ Nieun Seo
sldmsdl@yuhs.ac

¹ Department of Radiology and Research Institute of Radiological Science, Severance Hospital, Yonsei University College of Medicine, 50-1 Yonsei-ro, Seodaemun-gu, Seoul 03722, Republic of Korea

² Department of Internal Medicine, Institute of Gastroenterology, Severance Hospital, Yonsei University College of Medicine, 50-1 Yonsei-ro, Seodaemun-gu, Seoul 03722, Republic of Korea

³ Department of Pathology, Severance Hospital, Yonsei University College of Medicine, 50-1 Yonsei-ro, Seodaemun-gu, Seoul 03722, Republic of Korea

DWI	Diffusion-weighted imaging
f	Perfusion fraction
HCC	Hepatocellular carcinoma
LSM	Liver stiffness measurement
MRE	Magnetic resonance elastography
TE	Transient elastography
USE	Ultrasound elastography

Introduction

Chronic liver disease accounts for approximately 3.5% of all deaths worldwide owing to complications of cirrhosis and hepatocellular carcinoma (HCC) [1]. While liver biopsy remains the gold standard for assessing hepatic fibrosis [2, 3], the significance of its results can be limited by sampling errors, and there is always the risk of complications due to its invasiveness. Moreover, although repeated assessment of hepatic fibrosis is becoming more important as recent studies suggest possible regression of fibrosis during treatment [4, 5], repeating liver biopsy is impractical in actual clinical practice.

With the recent advances in imaging techniques, several noninvasive methods have been explored for diagnosing liver fibrosis including ultrasound elastography (USE), magnetic resonance elastography (MRE), and diffusion-weighted imaging (DWI) [6–10]. Among the USE techniques, transient elastography (TE) is the most widely used and validated technique [11–13]. It is rapid and user-friendly enabling almost immediate results with good reproducibility [11]. Among the MR techniques, MRE shows the highest diagnostic accuracy for liver fibrosis, but high cost and requirements for additional hardware and commercially available software are some of its disadvantages.

DWI using the mono-, bi-, and stretched exponential models have also been explored for staging hepatic fibrosis [7, 14, 15]. The stretched exponential model can reflect physiological characteristics in vivo tissue without restriction of the number of tissue compartmentalization, in contrast to the two compartments of the biexponential model [7, 16]. Compared with the mono- and biexponential models, there have been fewer studies on the stretched exponential model for liver fibrosis, including a previous study that showed better performance of the stretched exponential model compared with the mono- and biexponential models [7]. However, no study has yet to compare the diagnostic performance of the stretched exponential model with TE. Additionally, although hepatic inflammation and steatosis are known to affect parameters in the mono- and biexponential DWI models [6, 10], no study has yet investigated the possible effect of these histopathologic findings on the stretched exponential model when assessing liver fibrosis.

Therefore, the purposes of this study were to compare the diagnostic performance of the stretched exponential DWI model with those of TE and the mono- and biexponential DWI models and to determine the influence of hepatic inflammation and steatosis on these DWI models and TE.

Materials and methods

Study population

This study was approved by our Institutional Review Board and written informed consent was waived due to its retrospective study design. From October 2015 to November 2018, 1296 adult patients who underwent liver dynamic MRI including DWI with multiple b values were screened. Most of the patients underwent liver MRI for evaluation of focal liver lesions. Patients who underwent both liver MRI and TE and had pathologic results of liver fibrosis were eligible for our study. The exclusion criteria were as follows (Fig. 1): (a) patients who did not undergo TE, (b) no pathologic results of the liver, (c) interval longer than 1 year between liver pathology and imaging, (d) patients who received right hemihepatectomy thus precluding region of interest (ROI) measurement of parameters, (e) iron deposition in liver pathology, and (f) chemotherapy-related sinusoidal obstruction in liver pathology. Patients with either one of these two pathology results were excluded because these factors are known to affect diffusion parameters [6, 17, 18]. We searched electronic medical records to collect data on patient demographics, underlying liver disease, laboratory findings, and body mass index for the above patients.

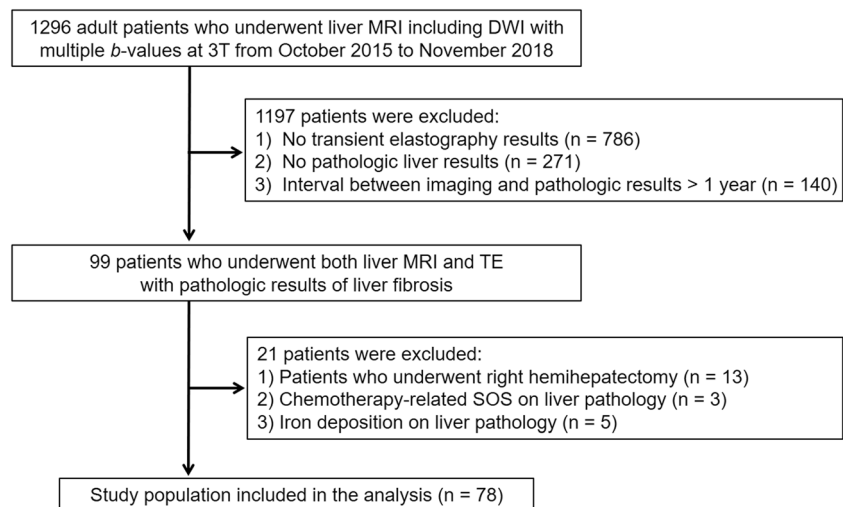
Transient elastography examination

Liver stiffness measurements (LSMs) were obtained using FibroScan® (Echosens) with a vibrator applied to the intercostal spaces at the level of the right hemiliver. LSM was expressed in kilopascals (kPa) and the median value was chosen to represent the elastic modulus of the liver. Interquartile range (IQR) was defined as an index of intrinsic variability for LSM, corresponding to the interval of LSM containing 50% of valid measurements between the 25th and 75th percentiles. LSMs with at least ten valid measurements with a success rate of at least 60% were considered reliable [19].

MR image acquisition

All images were acquired using a 3-T MR scanner (Achieva TX or Ingenia; Philips Healthcare) with anterior and posterior coils. The routine liver dynamic MRI

Fig. 1 Study flow diagram. MRI, magnetic resonance imaging; DWI, diffusion-weighted imaging; TE, transient elastography; SOS, sinusoidal obstruction syndrome



protocol consisted of noncontrast T1-weighted and T2-weighted images, DWI, and contrast-enhanced T1-weighted images. DWI was obtained using free-breathing, fat-suppressed single-shot echo-planar imaging with the following parameters: echo time, 50.2 ms; repetition time, 5000 ms; echo train length, 27; receiver bandwidth, 2877 per pixel; field of view, 400 mm; matrix size, 90×92 ; number of excitation, 3; section thickness, 5 mm; spectral adiabatic inversion-recovery fat suppression; and acquisition time, approximately 4 min 15 s. Three orthogonal spatial directions were encoded with nine diffusion-weighted gradients using the b values of 0, 10, 25, 50, 75, 100, 200, 500, and 800 s/mm^2 .

Postprocessing and image analysis of diffusion-weighted MRI

DWI data were analyzed using a postprocessing software (EXPRESS; Philips Healthcare) which was developed for research purposes, and DWI parameters and parametric maps were acquired.

The ADC value was calculated using the monoexponential linear fitting (least-square) technique (i.e., monoexponential model) with all nine b values according to the following equation:

$$S(b)/S(0) = \exp(-b \cdot \text{ADC})$$

where b is the b factor applied in DWI, $S(b)$ is the signal intensity at a given b value, and $S(0)$ is the signal intensity in the absence of any diffusion weighting.

In the case of the biexponential model, the true diffusion coefficient (D_t) was calculated using b values $> 200 \text{ s/mm}^2$ with the simple linear fit equation. The pseudodiffusion

coefficient (D_p) and perfusion fraction (f) were then obtained via a nonlinear regression algorithm [20]:

$$S(b)/S(0) = [(1-f) \cdot \exp(-b \cdot D_t)] + [f \cdot \exp(-b \cdot D_p)]$$

Likewise, in the stretched exponential model, the distributed diffusion coefficient (DDC) and intravoxel heterogeneity index (α) were calculated via the following equation [16]:

$$S(b)/S(0) = \exp[-(b \cdot \text{DDC})^\alpha]$$

Here, DDC represents the mean intravoxel diffusion rate and α represents the intravoxel water molecular diffusion heterogeneity which ranges from 0 to 1. To evaluate the diagnostic performance of DDC and α using abbreviated b values (0, 50, 500, 800 s/mm^2) generally covered in liver MRI, DDC and α using these four b values were also calculated and are herein defined as DDC^a and α^a . Using the postprocessing software, diffusion parameters were calculated using selected b values for the same ROIs with the full b -value imaging set. For both biexponential and stretched exponential models, the Levenberg–Marquardt fit was used [21].

Two radiologists, one board-certified abdominal radiologist with 8 years of experience in liver MRI and one junior radiology resident, performed image analyses independently. They were blinded to clinicopathologic findings and ROIs were drawn on DWI images ($b = 0 \text{ s/mm}^2$) using the postprocessing software. Three circular ROIs were drawn in different locations on the right hemiliver while avoiding large intrahepatic vessels and focal hepatic lesions. The left hemiliver and right liver dome were avoided as measurements could be unreliable from cardiac motion artifacts [22]. The mean area of the ROIs was $335.0 \pm 105.2 \text{ mm}^2$. The six ROI values attained by the two reviewers were used to analyze

variability according to liver location and to calculate interobserver agreements for diffusion parameters. The average of the six ROI values was used for other statistical analyses.

Histopathological analysis

Pathological assessment was used as the reference standard. The mean time interval between the date of imaging studies and pathologic diagnosis was 34.5 ± 98.1 days for MRI and 94.5 ± 181.2 days for TE. Pathologic specimens were obtained via hepatic resection ($n = 69$), percutaneous liver biopsy ($n = 6$), and transplantation ($n = 3$). The degree of fibrosis, steatosis, and inflammation were assessed according to the METAVIR and steatosis, activity, and fibrosis (SAF) scoring systems [23, 24]. Fibrosis was staged as follows: F0, no fibrosis; F1, periportal fibrosis without septa; F2, periportal fibrosis with few septa; F3, septal fibrosis; and F4, cirrhosis. Hepatic steatosis was scored from 0 to 3 via visual assessment of the percentage of hepatocytes presenting large- or medium-sized fatty droplets as follows: S0, < 5%; S1, 5–33%; S2, 34–66%; and S3, > 67%. Inflammatory activity was graded as follows: A0, no activity; A1, mild activity; A2, moderate activity; and A3, severe activity.

Statistical analysis

Continuous variables are expressed as means \pm standard deviations, while categorical variables are expressed as number of cases and percentages. TE and DWI parameters were compared between patients with F0–1, F2–3, and F4 using the one-way analysis of variance (ANOVA) test. Before the ANOVA test, data were tested for normal distribution using the Kolmogorov–Smirnov test. Post hoc analysis with Bonferroni multiple comparisons was performed for pairwise comparisons between each fibrosis group. The influence of histologic fibrosis, inflammation, and steatosis to the imaging parameters was determined by Spearman's rank correlation and multiple regression analysis. Spearman's rank correlation coefficient ρ ranges from -1 to $+1$ with the absolute value representing the strength of the correlation (0, no correlation; 0.2, weak correlation; 0.5, moderate correlation; 0.8, strong correlation; 1, perfect correlation) [25]. After confirming correlation, a stepwise multiple regression analysis with conditional backward elimination was performed to determine independent predictors for imaging parameters. Standardized coefficients called β weights and coefficients of determination (R^2) were reported for each parameter. Variance inflation factors (VIFs) were calculated to evaluate the effect of collinearity between independent factors. A VIF greater than 10 indicated the presence of multicollinearity.

The overall diagnostic performances of TE and DWI parameters for staging liver fibrosis were evaluated using the

Obuchowski measure [26], and the measures were compared between different parameters using the De Long test. The Obuchowski measure is a generalization of the area under the receiver-operating characteristic curve that can be used when a reference standard is multinomial [26]. Post hoc analysis with Bonferroni multiple comparisons was performed for pairwise comparisons between each parameter. The reliability of the DWI parameters was evaluated using the coefficient of variation (CoV) and intraclass correlation coefficients (ICC). Intraindividual variability among the six ROIs in the liver was calculated with CoV. Interreader agreement for ROI measurements between the two readers was assessed with ICC. ICC values of ≥ 0.75 indicate excellent agreement; 0.60–0.74, good; 0.40–0.59, fair; and < 0.40 , poor [27]. Analyses were performed using R package version 3.6.0 (R Foundation for Statistical Computing), MedCalc version 19.0.7 (MedCalc Software), and SPSS software version 25.0. P values < 0.05 were considered statistically significant.

Results

Patient characteristics

Based on the aforementioned criteria, a total of 78 patients (mean age, 58 ± 10 years; 62 men) were found eligible for our study (Fig. 1). Clinical and histopathologic findings of the patients are summarized in Table 1. Of the 78 patients, 63 (80.8%) had underlying liver disease, and the most common etiology was chronic hepatitis B (64.1%, 50/78). Sixteen (20.5%) patients had serum alanine aminotransferase levels more than two times higher than the normal upper limit. Regarding pathologic liver fibrosis, 12, 7, 6, 21, and 32 patients had F0, F1, F2, F3, and F4, respectively. Most patients had hepatic malignancy (96.2%, 75/78) with the malignancies being diagnosed as hepatocellular carcinoma (HCC) ($n = 56$), metastasis ($n = 14$), cholangiocarcinoma ($n = 2$), combined HCC and cholangiocarcinoma ($n = 1$), adult-type hepatoblastoma ($n = 1$), and leukemic involvement ($n = 1$).

Imaging parametric values according to the stage of hepatic fibrosis

LSM values obtained using TE and DWI parameters according to fibrosis stage are summarized in Table 2 and Figs. 2, 3, and 4. TE ($p < 0.001$), ADC ($p = 0.007$), f ($p = 0.042$), DDC ($p < 0.001$), and DDC^a ($p < 0.001$) values were significantly different between the F0–1, F2–3, and F4 stages. Among these parameters, all parameters except f were significantly different between F2–3 and F4 ($ps \leq 0.043$). However, only DDC was significantly different between F0–1 (1.272 \pm 0.177) and F2–3 (1.067 \pm 0.124; $p < 0.001$).

Table 1 Clinical–pathologic characteristics of 78 patients

Characteristics	Value
Age (years)	58 ± 10
Sex	
Men	62 (79.5)
Women	16 (20.5)
Underlying liver disease	
Chronic HBV infection	50 (64.1)
Chronic HCV infection	6 (7.7)
Chronic alcoholic liver disease	6 (7.7)
Autoimmune liver disease	1 (1.3)
No chronic liver disease	15 (19.2)
Laboratory findings	
Aspartate aminotransferase (IU/L)	46.6 ± 67.0
Alanine aminotransferase (IU/L)	45.9 ± 83.7
Total bilirubin (mg/dL)	0.8 ± 0.6
Alkaline phosphatase (IU/L)	79.4 ± 33.1
Gamma-glutamyl transferase (U/L)	46.9 ± 38.8
Platelet ($10^3/\mu\text{L}$)	173.9 ± 62.0
Body mass index (kg/m^2)	24.2 ± 3.1
Liver pathology	
Fibrosis	
F0	12 (15.4)
F1	7 (9.0)
F2	6 (7.7)
F3	21 (26.9)
F4	32 (41.0)
Inflammatory activity	
A0	12 (15.4)
A1	10 (12.8)
A2	54 (69.2)
A3	2 (2.6)
Steatosis	
S0	43 (55.1)
S1	29 (37.2)
S2	6 (7.7)
S3	0 (0.0)

Data in parentheses are percentages. Continuous variables are presented as mean ± standard deviation

HBV, hepatitis B virus, HCV, hepatitis C virus

Influence of hepatic fibrosis, inflammation, and steatosis on transient elastography and diffusion parameters

TE showed a significant positive correlation ($\rho = 0.539$, $p < 0.001$) with hepatic fibrosis. DWI parameters except D_p , α , and α^a also showed a significant correlation with fibrosis (Table 3). DDC had the strongest negative correlation ($\rho = -0.639$, $p < 0.001$) followed by DDC^a ($\rho = -0.496$,

$p < 0.001$) and ADC ($\rho = -0.343$, $p = 0.002$). For hepatic inflammation, TE ($\rho = 0.459$, $p < 0.001$), DDC ($\rho = -0.363$, $p = 0.001$), and DDC^a ($\rho = -0.324$, $p = 0.004$) showed a significant correlation with inflammatory activity. As for hepatic steatosis, the three DWI parameters ADC ($\rho = -0.325$, $p = 0.004$), D_p ($\rho = 0.267$, $p = 0.029$), and D_t ($\rho = -0.236$, $p = 0.038$) showed significant correlation. DDC ($p = 0.619$) and TE ($p = 0.057$) did not show a significant correlation with steatosis.

In the multiple regression analysis, fibrosis was the only independent factor associated with TE ($\beta = 2.981$, $p = 0.001$), DDC ($\beta = -0.114$, $p < 0.001$), and DDC^a ($\beta = -0.071$, $p < 0.001$). On the other hand, only steatosis was significantly associated with D_p ($\beta = 15.233$, $p = 0.029$), while both fibrosis and steatosis were associated with ADC ($p = 0.001$ for both fibrosis and steatosis) and D_t ($p = 0.020$ and $p = 0.007$).

Diagnostic performance of transient elastography and diffusion parameters for staging liver fibrosis

DDC had the highest Obuchowski measure for staging liver fibrosis (0.717; 95% CI, 0.653–0.765) followed by TE (0.681, 0.623–0.733), DDC^a (0.663, 0.599–0.719), and ADC (0.608, 0.543–0.671) (Table 4). DDC showed a significantly better performance than ADC ($p = 0.032$), f ($p < 0.001$), D_p ($p = 0.014$), D_t ($p = 0.015$), α ($p < 0.001$), and α^a ($p < 0.001$). However, there were no significant differences between DDC and TE ($p > 0.999$) and between DDC and DDC^a ($p = 0.473$).

Reliability of TE and diffusion parameters

Reliability of TE was evaluated by the IQR/median ratio (IQR/med) of the LSM values. The median IQR/med value was 13 (range, 0–26), indicating reliable examinations. The reliability of the DWI parameters was assessed using CoV and ICC (Table 5). Higher CoV values indicate higher variability of DWI parameters among the different locations of the liver. CoV was lowest for ADC (12.5%) followed by DDC (17.2%), D_t (18.2%), and DDC^a (21.0%). On the other hand, CoV was highest for perfusion-related parameters, including D_p (61.0%) and f (27.4%). Interreader agreement for DWI analysis between the two reviewers was good to excellent (ICC, 0.733–0.848).

Discussion

Our results showed that DDC from the stretched exponential DWI model showed the best diagnostic performance for staging liver fibrosis, followed by TE, although the difference between the two was not significant. Moreover, only DDC could differentiate both between F0–1 and F2–3 and between F2–3 and F4. DDC as well as TE was significantly correlated with hepatic fibrosis and inflammation, but fibrosis was the only independent factor for DDC and TE. In addition,

Table 2 Values of TE and DWI parameters according to the hepatic fibrosis stage

Modality	Parameter	F0–1 (n = 19)	F2–3 (n = 27)	F4 (n = 32)	p value*
Transient elastography	LSM (kPa)	5.442 ± 1.419	8.030 ± 3.429	17.163 ± 16.963	< 0.001
Monoexponential DWI	ADC (10 ⁻³ mm ² /s)	1.275 ± 0.105	1.255 ± 0.108	1.186 ± 0.106	0.007
Biexponential DWI	f (%)	26.478 ± 1.455	25.921 ± 6.548	22.743 ± 5.832	0.042
	D _p (10 ⁻³ mm ² /s)	105.623 ± 56.437	102.593 ± 30.106	88.349 ± 32.667	0.224
	D _t (10 ⁻³ mm ² /s)	0.976 ± 0.116	0.938 ± 0.106	0.897 ± 0.155	0.112
Stretched exponential DWI	DDC (10 ⁻³ mm ² /s)	1.272 ± 0.177	1.067 ± 0.124	0.954 ± 0.144	< 0.001
	α	0.494 ± 0.104	0.449 ± 0.111	0.494 ± 0.085	0.168
	DDC ^a (10 ⁻³ mm ² /s)	1.315 ± 0.190	1.194 ± 0.175	1.051 ± 0.174	< 0.001
	α ^a	0.508 ± 0.101	0.458 ± 0.114	0.515 ± 0.107	0.113

Data are means ± standard deviations

TE, transient elastography; DWI, diffusion-weighted imaging; LSM, liver stiffness measurement; ADC, apparent diffusion coefficient; f, perfusion fraction; D_p, pseudodiffusion coefficient; D_t, true diffusion coefficient; DDC, distributed diffusion coefficient; α, intravoxel diffusion heterogeneity index; DDC^a, DDC obtained using a four b-value dataset; α^a, α obtained using a four b-value dataset

* p values were obtained from comparisons between F0–1, F2–3, and F4

steatosis was not associated with stretched exponential DWI
 TE, but associated with ADC, D_p, and D_t.

A stretched exponential model reflects non-Gaussian molecular diffusion and represents the degree of intravoxel

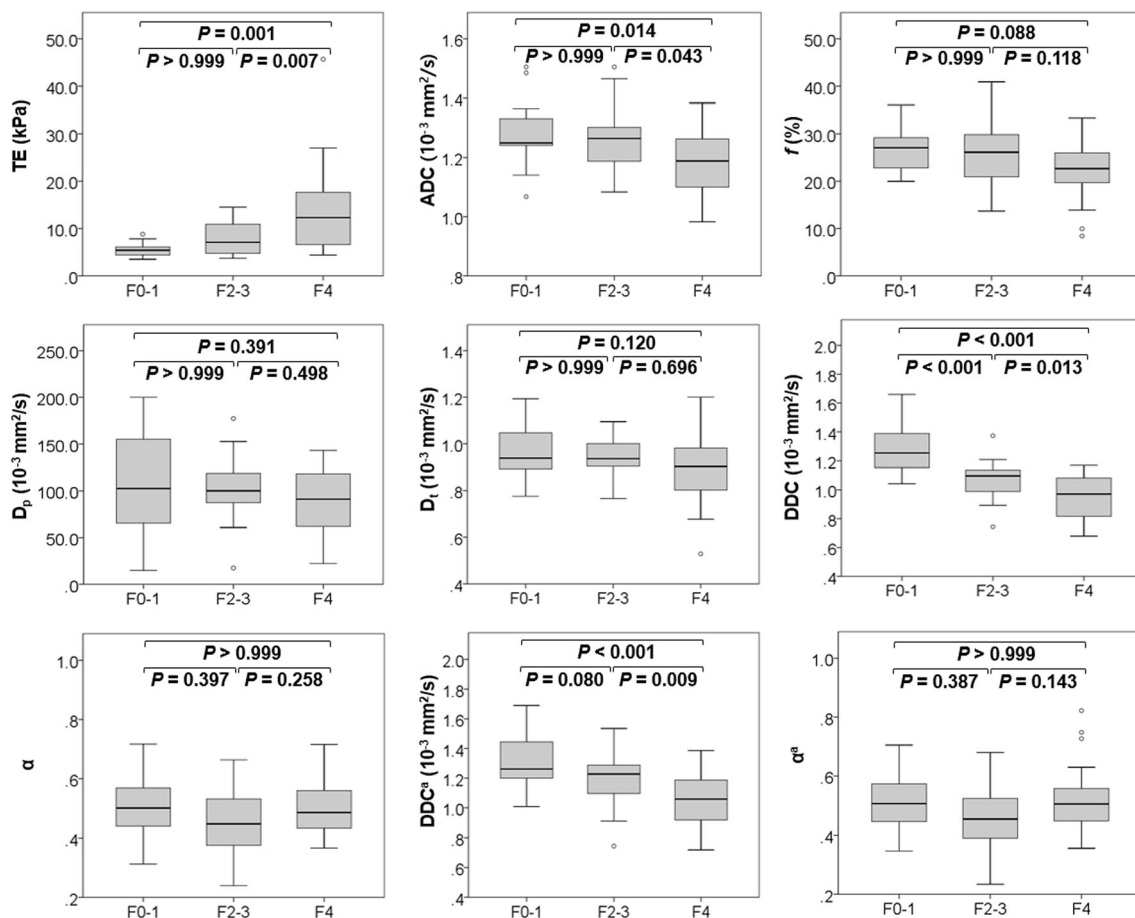


Fig. 2 Box plots of transient elastography (TE) and diffusion-weighted imaging parameters according to fibrosis stage (F0–1, F2–3, and F4). DDC was the only parameter to show significant difference between F0–1 and F2–3 and between F2–3 and F4. ADC, apparent diffusion

coefficient; f, perfusion fraction; D_p, pseudodiffusion coefficient; D_t, true diffusion coefficient; DDC, distributed diffusion coefficient; α, intravoxel diffusion heterogeneity index; DDC^a, DDC obtained using a four b-value dataset; α^a, α obtained using a four b-value dataset

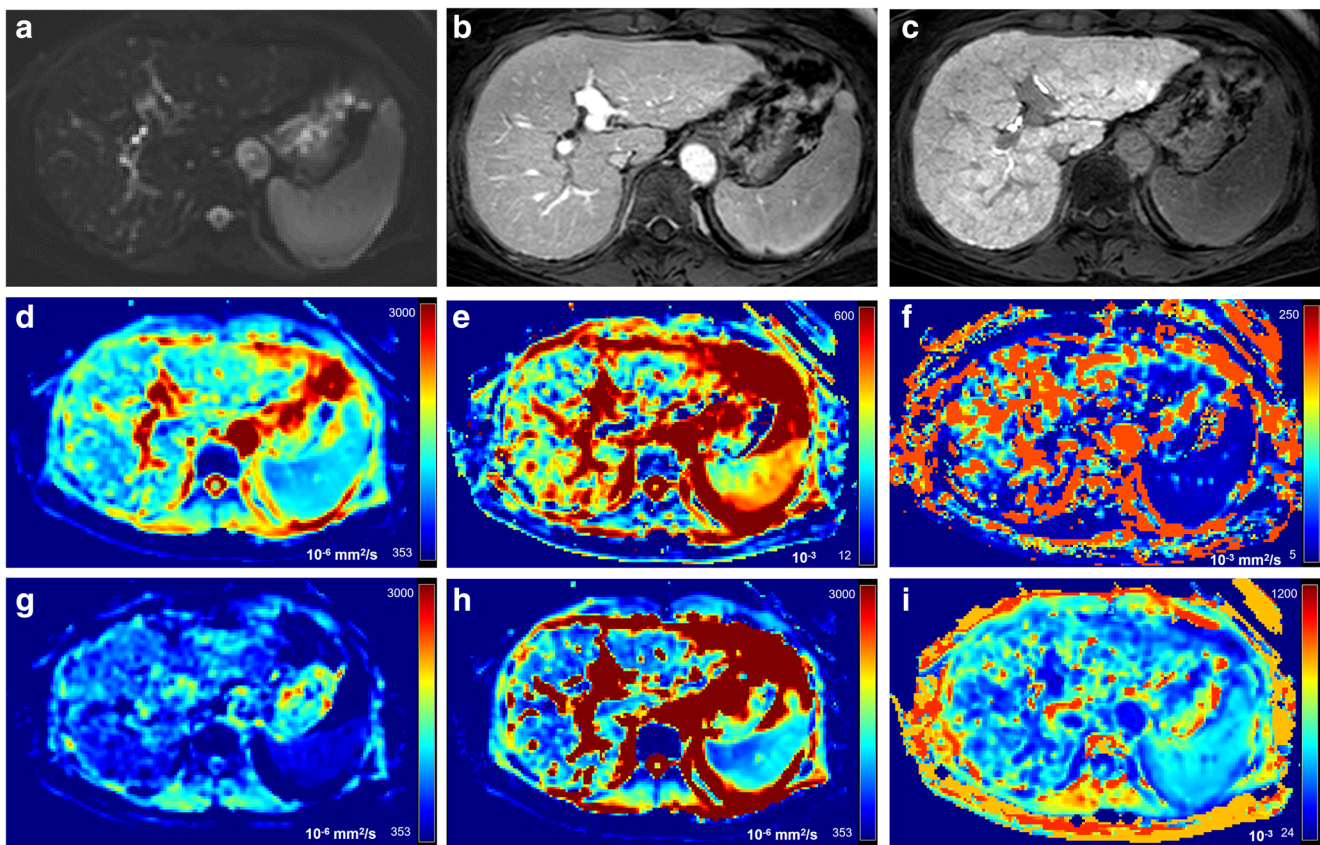


Fig. 3 Images of liver cirrhosis in a 67-year-old woman. **a** A native image acquired with a b value of 0 s/mm^2 . **b** A portal venous phase T1-weighted image. **c** A hepatobiliary phase image shows a cirrhotic liver. Parametric maps of **d** ADC ($10^{-6} \text{ mm}^2/\text{s}$), **e** f (10^{-3}), **f** D_p ($10^{-3} \text{ mm}^2/\text{s}$), **g** D_t (10^{-6}

mm^2/s), **h** DDC ($10^{-6} \text{ mm}^2/\text{s}$), and **i** α (10^{-3}) are shown. Liver stiffness measurement by transient elastography was 16.3 kPa. Results of liver pathology were F4 (cirrhosis), A2 (moderate inflammatory activity), and S0 (no steatosis)

heterogeneity of biological tissue [7, 16]. Consistent with a previous study [7], DDC from the stretched exponential model showed significantly better diagnostic performance for staging liver fibrosis than both the mono- and biexponential DWI models. DDC, which represents a continuous distribution of diffusion coefficients from different diffusion compartments, seems to reflect the degree of liver fibrosis more accurately than the mono- or biexponential DWI models. DDC also showed smaller CoV than parameters from the biexponential DWI, indicating less variability across different liver locations. On the other hand, α , another parameter from the stretched exponential model which reflects intravoxel diffusion heterogeneity, did not show a significant correlation with fibrosis in this study. Previous studies have shown inconsistent results for the association between α and hepatic fibrosis [7, 28]. An animal study showed no significant correlation between α and hepatic fibrosis [28], whereas another human study reported that α as well as DDC had a significant negative correlation with fibrosis [7]. While the presence of more connective tissues, narrowing of sinusoids, and decreased blood flow may explain architectural heterogeneity in the fibrotic liver, these changes may not aggravate heterogeneity in advanced fibrosis stages [29, 30]. Also, the larger proportion

of patients with no or early stage fibrosis (F0–1) included in the previous study (44/95, 46.3%) compared with our study (19/78, 24.4%) may have contributed to the discordant study results. Further larger studies are warranted to validate the role of α in hepatic fibrosis.

Regarding the diagnostic performance of TE and MRI for staging liver fibrosis, TE has been reported to be less accurate than MRE parameters, but comparable to the biexponential DWI models [10, 12, 31]. Our results showed that DDC has good diagnostic performance comparable to TE. Of note, unlike TE, DDC could differentiate between F0–1 and F2–3, as well as between F2–3 and F4. TE is reported to be less effective when identifying early-stage fibrosis [9, 10]. In addition, the diagnostic performance of DDC^a using four abbreviated b values (0, 50, 500, 800 s/mm^2) was also evaluated because DWI using fewer b values can reduce scanning time. Although the diagnostic performance of DDC^a for staging liver fibrosis was slightly lower than DDC, the difference was not significant between DDC^a and DDC. Considering the disadvantages of TE including operator dependency, restrictions on its use in patients with ascites or obesity, and the inability to evaluate the background liver or focal liver lesion, the stretched exponential DWI model using

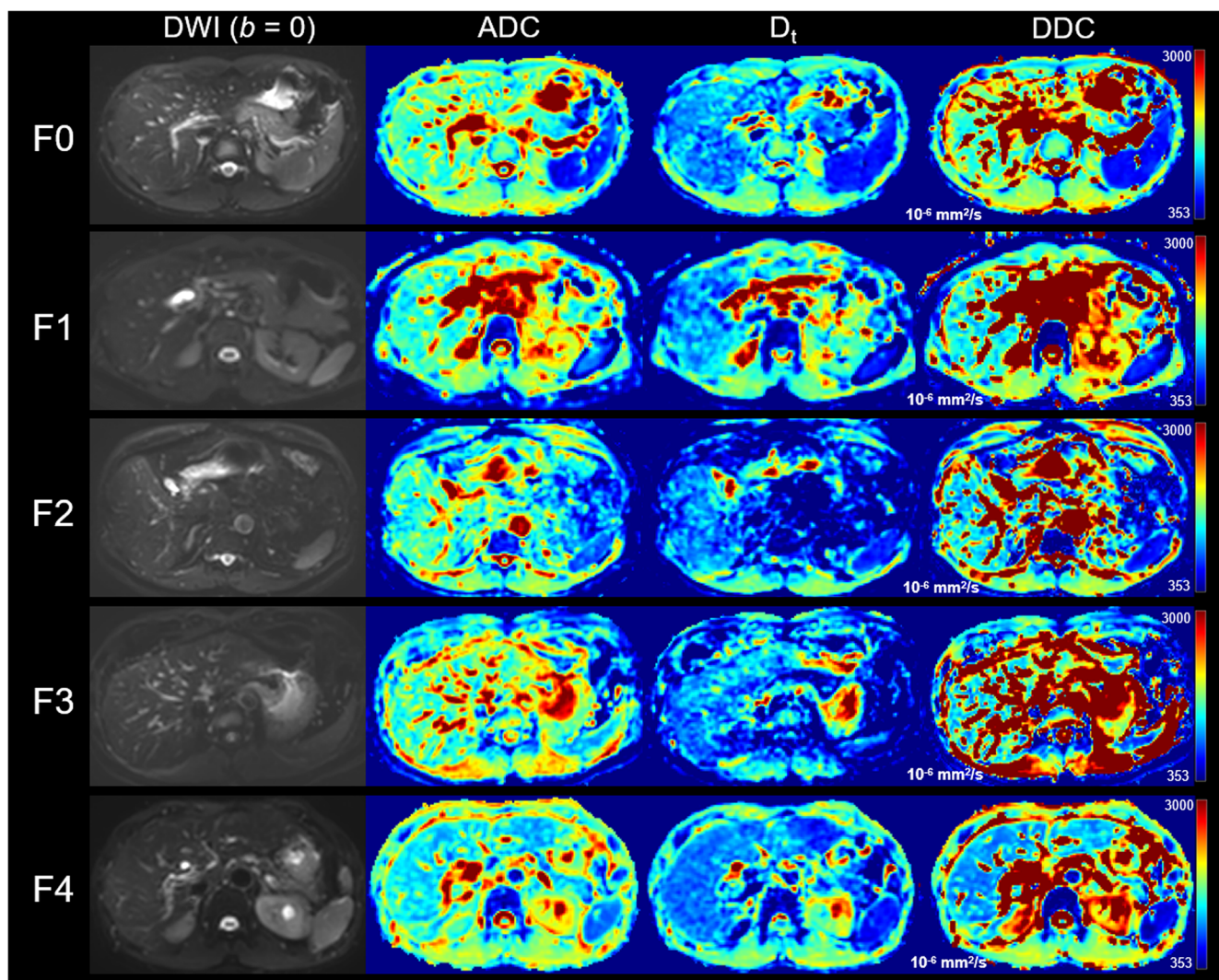


Fig. 4 DWI ($b = 0$ s/mm²), ADC (10^{-6} mm²/s), D_t (10^{-6} mm²/s), and DDC (10^{-6} mm²/s) maps comparing different degrees of hepatic fibrosis. DDC maps show values decrease with the progression of liver fibrosis: 1.659, 1.435, 1.227, 1.108, and 1.020 (10^{-3} mm²/s) for patients with F0, F1, F2, F3, and F4, respectively. Liver stiffness measured by transient

elastography was 5.4 kPa, 4.6 kPa, 11.8 kPa, 10.5 kPa, and 9.5 kPa for patients with F0, F1, F2, F3, and F4, respectively. DWI, diffusion-weighted imaging; ADC, apparent diffusion coefficient; D_t , true diffusion coefficient; DDC, distributed diffusion coefficient

abbreviated b values can be easily applied to the evaluation of fibrosis even in patients who undergo routine liver MRI without additional scan time.

Several different methods can be used for curve fitting in nonmonoexponential DWI models, and the chosen fitting method can affect the accuracy and reliability of the models. In this study, the Levenberg–Marquardt algorithm (LMA) was used for the biexponential and stretched exponential models. It is commonly used for nonlinear least-square fitting and has been applied for biexponential model fitting in previous studies [21, 32, 33]. LMA identifies parameters which best fit the datasets using iterative minimization. LMA requires an initial guess which acts as a stepping stone for the process of iterative minimization to begin on, and the chosen initial value affects the accuracy of the parameters. In our study, instead of using

fixed initial values, initial values roughly calculated pixel by pixel from the actual required dataset were used. By using calculated initial values that had the same physical significance as the actual fitting results, the quality of the overall map improved with a better chance of accurate fitting. For IVIM analysis, we used segmented fitting instead of fully unconstrained free fitting. The segmented IVIM analysis used in this study with its precalculations of D_t can improve the mathematical stability of the results by reducing the degree of freedom during the fitting process.

This study investigated the possible confounding factors of the stretched exponential model for evaluating fibrosis. DDC showed a significant correlation with hepatic fibrosis and inflammation but not with steatosis. In the multiple regression analysis, fibrosis was the only independent

Table 3 Correlation and multiple regression analyses: influence of hepatic fibrosis, inflammation, and steatosis on the imaging parameters

	Correlation analysis		Multiple regression analysis			
	Spearman's ρ	p value	p value	R^2	β value	95% CI of β
TE (kPa)						
Fibrosis	0.539	< 0.001	0.001	0.131	2.981	1.227, 4.735
Inflammation	0.459	< 0.001	0.632			
Steatosis	0.216	0.057				
ADC (10^{-3} mm ² /s)						
Fibrosis	- 0.343	0.002	0.001	0.235	- 0.028	- 0.043, - 0.013
Inflammation	- 0.147	0.198				
Steatosis	- 0.325	0.004	0.001	0.235	- 0.060	- 0.096, - 0.025
f (%)						
Fibrosis	- 0.247	0.029				
Inflammation	- 0.057	0.620				
Steatosis	- 0.009	0.935				
D_p (10^{-3} mm ² /s)						
Fibrosis	- 0.159	0.163				
Inflammation	- 0.015	0.895				
Steatosis	0.267	0.029	0.029	0.062	15.233	1.640, 28.825
D_t (10^{-3} mm ² /s)						
Fibrosis	- 0.236	0.038	0.020	0.143	- 0.023	- 0.042, - 0.001
Inflammation	- 0.192	0.091				
Steatosis	- 0.236	0.038	0.007	0.143	- 0.062	- 0.107, - 0.018
DDC (10^{-3} mm ² /s)						
Fibrosis	- 0.639	< 0.001	< 0.001	0.468	- 0.114	- 0.151, - 0.076
Inflammation	- 0.363	0.001	0.082			
Steatosis	- 0.057	0.619				
α						
Fibrosis	0.033	0.777				
Inflammation	- 0.181	0.114				
Steatosis	0.051	0.655				
DDC ^a (10^{-3} mm ² /s)						
Fibrosis	- 0.496	< 0.001	< 0.001	0.256	- 0.071	- 0.098, - 0.043
Inflammation	- 0.324	0.004	0.862			
Steatosis	- 0.055	0.633				
α^a						
Fibrosis	0.049	0.670				
Inflammation	- 0.153	0.182				
Steatosis	0.012	0.919				

DWI, diffusion-weighted imaging; CI, confidence interval; ADC, apparent diffusion coefficient; f , perfusion fraction; D_p , pseudodiffusion coefficient; D_t , true diffusion coefficient; DDC, distributed diffusion coefficient; α , intravoxel diffusion heterogeneity index; DDC^a, DDC obtained using a four b -value dataset; α^a , α obtained using a four b -value dataset

factor associated with DDC. Inflammation may increase liver stiffness value by increasing cellularity, cell size, or hydrostatic pressure [34]. However, the effect of inflammation on DDC was weaker than fibrosis in this study, and no independent association was identified between inflammation and DDC. Regarding the other DWI models, both steatosis and fibrosis were independently associated with

ADC and D_t , which is generally consistent with previous reports [6, 35, 36]. Although most patients in our study were categorized as having no or mild steatosis (55.1% and 37.2%, respectively), the effect of steatosis on ADC and D_t was significant, indicating a confounding effect of even mild steatosis on the mono- and biexponential DWI models.

Table 4 Overall diagnostic performance for staging liver fibrosis

	Parameter	Obuchowski measures	95% CI	<i>p</i> value*
TE	LSM (kPa)	0.681	0.623–0.733	> 0.999
Monoexponential DWI	ADC (10^{-3} mm ² /s)	0.608	0.543–0.671	0.032
Biexponential DWI	<i>f</i> (%)	0.576	0.516–0.633	< 0.001
	<i>D_p</i> (10^{-3} mm ² /s)	0.553	0.493–0.632	0.014
	<i>D_t</i> (10^{-3} mm ² /s)	0.573	0.506–0.657	0.015
Stretched exponential DWI	DDC (10^{-3} mm ² /s)	0.717	0.653–0.765	NA
	α	0.488	0.479–0.588	< 0.001
	DDC ^a (10^{-3} mm ² /s)	0.663	0.599–0.719	0.473
	α^a	0.519	0.480–0.591	< 0.001

TE, transient elastography; DWI, diffusion-weighted imaging; CI, confidence interval; LSM, liver stiffness measurement; ADC, apparent diffusion coefficient; *f*, perfusion fraction; *D_p*, pseudodiffusion coefficient; *D_t*, true diffusion coefficient; DDC, distributed diffusion coefficient; α , intravoxel diffusion heterogeneity index; DDC^a, DDC obtained using a four *b*-value dataset; α^a , α obtained using a four *b*-value dataset; NA, not applicable

* *p* values were obtained from comparisons of DDC and other parameters

This study has several limitations. First, this study has an inherent selection bias due to its retrospective design. While the etiology of chronic liver disease was diverse, most of the patients had chronic hepatitis B. In addition, the number of patients with each grade of fibrosis, steatosis, and inflammation was not even, as relatively large portions of patients had advanced fibrosis and no or mild steatosis. Second, the time interval between imaging and pathology confirmation was relatively long. Third, discrepancies may exist between the locations of the ROI measurements for TE or DWI models and pathologic evaluation, and this might have caused potential bias as hepatic fibrosis can be heterogeneously distributed. Finally, the abbreviated *b* values of the imaging set of the stretched exponential model was calculated by arbitrarily selecting four *b* values,

Table 5 Reliability of DWI analysis

	CoV (%)	95% CI of CoV	ICC	95% CI of ICC
ADC	12.5	10.7–14.9	0.733	0.581–0.829
<i>f</i>	27.4	23.5–33.0	0.816	0.711–0.882
<i>D_p</i>	61.0	50.6–77.2	0.774	0.647–0.856
<i>D_t</i>	18.2	15.7–21.9	0.769	0.639–0.853
DDC	17.2	14.8–20.6	0.771	0.641–0.854
α	22.7	19.5–27.2	0.848	0.763–0.903
DDC ^a	21.0	18.1–25.1	0.781	0.657–0.860
α^a	23.7	20.3–28.4	0.804	0.694–0.875

Variability of DWI values according to different liver locations was evaluated by CoV (%), whereas interobserver agreement between the two reviewers was evaluated by ICC

DWI, diffusion-weighted imaging; CoV, coefficient of variation; ICC, intraclass correlation coefficient; CI, confidence interval; ADC, apparent diffusion coefficient; *f*, perfusion fraction; *D_p*, pseudodiffusion coefficient; *D_t*, true diffusion coefficient; DDC, distributed diffusion coefficient; α , intravoxel diffusion heterogeneity index; DDC^a, DDC obtained using a four *b*-value dataset; α^a , α obtained using a four *b*-value dataset

generally included in the routine liver MRI protocol. Further prospective studies are needed to evaluate the optimal number and composition of *b* values for the stretched exponential model.

In conclusion, DDC from the stretched exponential model is the most accurate DWI parameter for staging liver fibrosis, with overall similar diagnostic performance to TE. Compared with other DWI models, the stretched exponential model seems more advantageous in the staging of liver fibrosis due to higher diagnostic performance, no confounding effects by steatosis, and better reliability.

Funding This study has received funding by a new faculty research seed money grant of Yonsei University College of Medicine for 2020 (2020-32-0040) and National Research Foundation of Korea (NRF) grant funded by the Korean government (MSIT) (No. NRF-2018R1C1B6002747).

Compliance with ethical standards

Guarantor The scientific guarantor of this publication is Nieuw Seo.

Conflict of interest The authors of this manuscript declare no relationships with any companies, whose products or services may be related to the subject matter of the article.

Statistics and biometry In Kyung Min (from the Biostatistics Collaboration Unit, Department of Biomedical Systems Informatics, Yonsei University College of Medicine) performed the statistical analyses.

Informed consent Written informed consent was waived by the Institutional Review Board of Yonsei University College of Medicine.

Ethical approval Institutional Review Board approval was obtained.

Methodology

- retrospective
- diagnostic or prognostic study
- performed at one institution

References

- Asrani SK, Devarbhavi H, Eaton J, Kamath PS (2019) Burden of liver diseases in the world. *J Hepatol* 70:151–171
- Chalalani N, Younossi Z, Lavine JE et al (2018) The diagnosis and management of nonalcoholic fatty liver disease: practice guidance from the American Association for the Study of Liver Diseases. *Hepatology* 67:328–357
- Terrault NA, Lok ASF, McMahon BJ et al (2018) Update on prevention, diagnosis, and treatment of chronic hepatitis B: AASLD 2018 hepatitis B guidance. *Hepatology* 67:1560–1599
- Chang TT, Liaw YF, Wu SS et al (2010) Long-term entecavir therapy results in the reversal of fibrosis/cirrhosis and continued histological improvement in patients with chronic hepatitis B. *Hepatology* 52:886–893
- Ellis EL, Mann DA (2012) Clinical evidence for the regression of liver fibrosis. *J Hepatol* 56:1171–1180
- Leitao HS, Doblaz S, Garteiser P et al (2017) Hepatic fibrosis, inflammation, and steatosis: influence on the MR viscoelastic and diffusion parameters in patients with chronic liver disease. *Radiology* 283:98–107
- Seo N, Chung YE, Park YN, Kim E, Hwang J, Kim MJ (2018) Liver fibrosis: stretched exponential model outperforms mono-exponential and bi-exponential models of diffusion-weighted MRI. *Eur Radiol* 28:2812–2822
- Petitclerc L, Sebastiani G, Gilbert G, Cloutier G, Tang A (2017) Liver fibrosis: review of current imaging and MRI quantification techniques. *J Magn Reson Imaging* 45:1276–1295
- Lefebvre T, Wartelle-Bladou C, Wong P et al (2019) Prospective comparison of transient, point shear wave, and magnetic resonance elastography for staging liver fibrosis. *Eur Radiol* 29:6477–6488
- Fu F, Li X, Chen C et al (2020) Non-invasive assessment of hepatic fibrosis: comparison of MR elastography to transient elastography and intravoxel incoherent motion diffusion-weighted MRI. *Abdom Radiol (NY)* 45:73–82
- Castera L, Forns X, Alberti A (2008) Non-invasive evaluation of liver fibrosis using transient elastography. *J Hepatol* 48:835–847
- Dyvorne HA, Jajamovich GH, Bane O et al (2016) Prospective comparison of magnetic resonance imaging to transient elastography and serum markers for liver fibrosis detection. *Liver Int* 36:659–666
- Zhang X, Wong GL, Wong VW (2020) Application of transient elastography in nonalcoholic fatty liver disease. *Clin Mol Hepatol* 26:128–141
- Yoon JH, Lee JM, Baek JH et al (2014) Evaluation of hepatic fibrosis using intravoxel incoherent motion in diffusion-weighted liver MRI. *J Comput Assist Tomogr* 38:110–116
- Chung SR, Lee SS, Kim N et al (2015) Intravoxel incoherent motion MRI for liver fibrosis assessment: a pilot study. *Acta Radiol* 56:1428–1436
- Bennett KM, Schmainda KM, Bennett RT, Rowe DB, Lu H, Hyde JS (2003) Characterization of continuously distributed cortical water diffusion rates with a stretched-exponential model. *Magn Reson Med* 50:727–734
- Bulow R, Mensel B, Meffert P, Hernando D, Evert M, Kuhn JP (2013) Diffusion-weighted magnetic resonance imaging for staging liver fibrosis is less reliable in the presence of fat and iron. *Eur Radiol* 23:1281–1287
- Zhang Q, Yu NN, Wen LJ et al (2012) A preliminary study of apparent diffusion coefficient in chemotherapy-induced liver damage. *Eur J Radiol* 81:2943–2946
- Kim SU, Han KH, Ahn SH (2010) Transient elastography in chronic hepatitis B: an Asian perspective. *World J Gastroenterol* 16:5173–5180
- Le Bihan D, Breton E, Lallemand D, Aubin ML, Vignaud J, Laval-Jeantet M (1988) Separation of diffusion and perfusion in intravoxel incoherent motion MR imaging. *Radiology* 168:497–505
- Bai Y, Lin Y, Tian J et al (2016) Grading of gliomas by using monoexponential, biexponential, and stretched exponential diffusion-weighted MR imaging and diffusion kurtosis MR imaging. *Radiology* 278:496–504
- Lee Y, Lee SS, Kim N et al (2015) Intravoxel incoherent motion diffusion-weighted MR imaging of the liver: effect of triggering methods on regional variability and measurement repeatability of quantitative parameters. *Radiology* 274:405–415
- Bedossa P, Poynard T (1996) An algorithm for the grading of activity in chronic hepatitis C. The METAVIR Cooperative Study Group. *Hepatology* 24:289–293
- Bedossa P, Poitou C, Veyrie N et al (2012) Histopathological algorithm and scoring system for evaluation of liver lesions in morbidly obese patients. *Hepatology* 56:1751–1759
- Zou KH, Tuncali K, Silverman SG (2003) Correlation and simple linear regression. *Radiology* 227:617–622
- Lambert J, Halfon P, Penaranda G, Bedossa P, Cacoub P, Carrat F (2008) How to measure the diagnostic accuracy of noninvasive liver fibrosis indices: the area under the ROC curve revisited. *Clin Chem* 54:1372–1378
- Hallgren KA (2012) Computing inter-rater reliability for observational data: an overview and tutorial. *Tutor Quant Methods Psychol* 8:23–34
- Anderson SW, Barry B, Soto J, Ozonoff A, O'Brien M, Jara H (2014) Characterizing non-Gaussian, high b-value diffusion in liver fibrosis: stretched exponential and diffusional kurtosis modeling. *J Magn Reson Imaging* 39:827–834
- Biagini G, Ballardini G (1989) Liver fibrosis and extracellular matrix. *J Hepatol* 8:115–124
- Standish RA, Cholongitas E, Dhillon A, Burroughs AK, Dhillon AP (2006) An appraisal of the histopathological assessment of liver fibrosis. *Gut* 55:569–578
- Park CC, Nguyen P, Hernandez C et al (2017) Magnetic resonance elastography vs transient elastography in detection of fibrosis and noninvasive measurement of steatosis in patients with biopsy-proven nonalcoholic fatty liver disease. *Gastroenterology* 152:598–607 e592
- Neil JJ, Bretthorst GL (1993) On the use of Bayesian probability theory for analysis of exponential decay data: an example taken from intravoxel incoherent motion experiments. *Magn Reson Med* 29:642–647
- Dyvorne HA, Galea N, Nevers T et al (2013) Diffusion-weighted imaging of the liver with multiple b values: effect of diffusion gradient polarity and breathing acquisition on image quality and intravoxel incoherent motion parameters—a pilot study. *Radiology* 266:920–929
- Iredale JP (2007) Models of liver fibrosis: exploring the dynamic nature of inflammation and repair in a solid organ. *J Clin Invest* 117:539–548
- Leitao HS, Doblaz S, d'Assignies G et al (2013) Fat deposition decreases diffusion parameters at MRI: a study in phantoms and patients with liver steatosis. *Eur Radiol* 23:461–467
- Guiu B, Petit JM, Capitan V et al (2012) Intravoxel incoherent motion diffusion-weighted imaging in nonalcoholic fatty liver disease: a 3.0-T MR study. *Radiology* 265:96–103

Publisher's note Springer Nature remains neutral with regard to jurisdictional claims in published maps and institutional affiliations.